Ca^{2+}-activated Cl^--currents are dispensable for olfaction

Gwendolyn M. Billig[1,§], Balázs Pál[1], Pawel Fidzinski[1] & Thomas J. Jentsch[1,2,*]

[1]Leibniz-Institut für Molekulare Pharmakologie (FMP) / Max-Delbrück-Centrum für Molekulare Medizin (MDC), Berlin, Germany

[2]NeuroCure Cluster of Excellence, Charité, Berlin, Germany

[§]Graduate student at the Freie Universität Berlin

[*] Corresponding author: Jentsch@fmp-berlin.de

Canonical olfactory signal transduction involves the activation of cAMP-activated cation channels that depolarize the cilia of receptor neurons and raise intracellular calcium. Calcium then activates Cl^- currents that may be up to tenfold larger than cation currents and are believed to powerfully amplify the response. We identified Anoctamin2 (Ano2, also known as TMEM16B) as the ciliary Ca^{2+}-activated Cl^- channel of olfactory receptor neurons. Ano2 is expressed in the main olfactory epithelium (MOE) and in the vomeronasal organ (VNO), which also expresses the related Ano1 channel. Disruption of *Ano2* in mice virtually abolished Ca^{2+}-activated Cl^- currents in the MOE and VNO. *Ano2* disruption reduced fluid-phase electro-olfactogram responses by only ~40%, did not change air-phase electro-olfactograms and did not reduce performance in olfactory behavioral tasks. In contrast with the current view, cyclic nucleotide–gated cation channels do not need a boost by Cl^- channels to achieve near-physiological levels of olfaction.

Olfaction in mammals involves the binding of odorants to a subset of the large number of different G protein–coupled receptors that are present in the cilia of olfactory sensory neurons (OSNs)[1]. These neurons are predominantly found in the MOE, which senses and discriminates myriad volatile compounds. In the mouse, the nose contains additional, apparently more specialized olfactory organs, such the septal organ of Masera and the VNO[2]. Sensory neurons in the VNO are morphologically distinct and use odorant receptors and signal transduction cascades that differ from those found in the MOE.

In the canonical OSN signal transduction pathway, odorant binding to the receptor locally increases cytosolic cAMP through activation of the olfactory G protein G_{olf} and adenylate cyclase type III[1,2]. cAMP then opens heteromeric cyclic nucleotide–gated (CNG) cation channels[3]. The resulting influx of Na^+ and Ca^{2+} depolarizes the plasma membrane and raises the cytosolic Ca^{2+} concentration ($[Ca^{2+}]_i$), thereby activating Ca^{2+}-activated Cl^- channels[1,4-10]. All these components of the signal transduction cascade are localized to sensory cilia, which are embedded in the mucus covering the MOE. These cilia provide a large interaction surface for odorants, and the cilia's small diameters facilitate large local increases in cytosolic cAMP and $[Ca^{2+}]$.

There has been broad consensus that Ca^{2+}-activated Cl^- channels powerfully amplify olfactory signal transduction[1,4-10]. These channels are thought to mediate an outward flow of Cl^-, which generates a depolarizing current that, in rodents, is five- to tenfold larger than currents through CNG channels[8,11,12]. A prerequisite for Cl^- efflux

is an inside-out electrochemical Cl^--gradient. It is believed that cytosolic chloride concentration of OSNs is raised by the $Na^+K^+2Cl^-$ co-transporter Nkcc1[9,10,13] and that [Cl^-] is low in the mucus surrounding the cilia [14,15]. However, mucosal ion concentrations are difficult to measure *in vivo*, and *Nkcc1* knockout mice display attenuated electro-olfactograms (EOGs)[11,16], but normal olfactory sensitivity[17].

To investigate the role of Ca^{2+}-activated Cl^- channels in olfaction, we disrupted *Ano2* in mice. *Ano2* is a member of the *Anoctamin* (*Tmem16)* gene family, which encodes several Ca^{2+}-activated Cl^- channels[18-20]. Agreeing with recent results[13,21-23], our knockout-controlled immunolabeling showed Ano2 expression in cilia of OSNs in the MOE, in microvilli of VNO sensory neurons and in synapses of photoreceptors. Additionally, we found Ano2 in the olfactory bulb. Ano1 expression overlapped with Ano2 in the VNO and the retina, but not in the MOE. Patch-clamp analysis showed that Ca^{2+}-activated Cl^- currents were undetectable in *Ano2*$^{-/-}$ OSNs. Unexpectedly, however, EOGs of *Ano2*$^{-/-}$ mice were reduced by only up to ~40%, and *Ano2*$^{-/-}$ mice were able to smell normally. Our work calls for a revision of the current view that Ca^{2+}-activated Cl^- channels have a crucial role in mammalian olfaction.

RESULTS

Disruption of *Ano2* and Ano2 expression pattern

We generated *Ano2*$^{-/-}$ mice by flanking exon 12 with loxP sites and crossing these mice with Cre-recombinase–expressing *deleter* mice[24] (**Supplementary Fig. 1a**,**b**). The ~160 kDa band that represents the Ano2 protein in *Ano2*$^{+/+}$ (wild-type) olfactory epithelium was absent from *Ano2*$^{-/-}$ tissue (**Fig. 1a**). Our N-terminal antibody did not detect a truncated protein in *Ano2*$^{-/-}$ tissue, suggesting the occurrence of nonsense-mediated mRNA decay, instability of the truncated protein, or both. *Ano2*$^{-/-}$ mice were born at Mendelian ratio; they grew, mated, and survived normally and lacked an immediately apparent phenotype.

Consistent with previous data[21-23], western blots indicated that Ano2 is most highly expressed in olfactory epithelium (MOE and VNO) and eye tissue (**Fig. 1a**,**b**). Ano2 was expressed at much lower levels in brain, with the highest expression in the olfactory bulb and signals near the detection limit in the midbrain and brainstem (**Fig. 1b**). We did not detect expression in the cortex, cerebellum or trigeminal nerve. The differences in apparent sizes of Ano2 among various tissues are due largely to a higher degree of glycosylation in olfactory tissues (**Supplementary Fig. 2**). Immunolabeling showed that Ano2 is expressed on the apical surface of both the MOE and the VNO (**Fig. 2a**). In the MOE, it colocalized with the cilia marker protein

acetylated tubulin (**Fig. 2b**) and the Cnga2 subunit of the olfactory CNG channel[3,25,26] (**Fig. 2c**). Ano2 staining was specific, as we observed no signal in *Ano2*$^{-/-}$ tissue (**Fig. 2c**).

We also detected Ano2 in vomeronasal sensory neurons (VSNs), where it colocalized with the closely related Ano1 Cl^- channel in sensory protrusions (**Fig. 3a**). In the MOE, however, we did not detect Ano1 in olfactory sensory neurons (**Fig. 3b**,**c**), but it was present in Bowman's glands (not shown). Similarly, Ano1 was present in the apical membranes of nasal glands (**Fig. 3b**,**d**) and in the non-ciliated cells of the respiratory epithelium (**Fig. 3b**–**d**), consistent with a role in salt secretion, as in other epithelia[18,27,28].

Ano2 protein was present on the OSN axons that converge on the glomeruli in the olfactory bulb (**Fig. 4a**,**b**). In the eye, our knockout-controlled staining confirmed the presence of Ano2 in the outer plexiform layer of the retina[22] (**Supplementary Fig. 3a**). Ano2 colocalized with the PSD-95 adaptor protein (**Supplementary Fig. 3b**) and the Ca^{2+}-ATPase PMCA (**Supplementary Fig. 3c**) in presynaptic structures of photoreceptors, where these proteins form a complex together with MPP4[22]. Whereas Ano2 is lost from photoreceptors of *Mpp4*$^{-/-}$ mice[22], loss of Ano2 affected neither PSD-95 nor PMCA expression (**Supplementary Fig. 3b**,**c**). Ano1 antibodies labeled the same structures that we had also identified as Ano2 positive (**Supplementary Fig. 3a**).

No change of key proteins and axonal convergence

Neither immunohistochemistry (**Fig. 3a**) nor immunoblotting (**Supplementary Fig. 4a**) indicated an upregulation of Ano1 in the VNO or MOE of *Ano2*$^{-/-}$ mice. Consistent with the normal morphology of both olfactory organs in *Ano2*$^{-/-}$ mice (**Figs. 2c** and **3a**), expression levels of the olfactory marker protein OMP[29] were unchanged (**Supplementary Fig. 4b**). *Ano2* disruption caused no change in expression of the downstream target of G_{olf}, adenylate cyclase III (**Supplementary Fig. 4c**,**f**), or of the cAMP-activated cation channel subunit Cnga2 (**Fig. 2c**, **Supplementary Fig. 4d**). Expression of Nkcc1, Ano6, Ano8, and Ano10 in the MOE was also unaltered (**Supplementary Fig. 4f**).

Immunohistochemistry (**Fig. 4a**) and immunoblotting (**Supplementary Fig. 4e**) showed no change in the amount of tyrosine hydroxylase in the olfactory bulb, either. The expression of this enzyme depends on neuronal activity and was severely reduced in the olfactory bulb of anosmic *Cnga2*$^{-/y}$ mice[30]. OSN axon coalescence on glomeruli is perturbed in mice lacking functional CNG channels[31] or the adenylate cyclase[32]. We detected no obvious change in axonal convergence for OSNs

expressing either the P2 or M72 receptor[31] (**Fig. 4c**–**e**). These observations suggest that olfaction is not grossly impaired in *Ano2*$^{-/-}$ mice and that intrinsic OSN activity is not changed to a degree that changes the olfactory map.

Ca^{2+}-activated Cl^- currents are absent from *Ano2*$^{-/-}$ OSNs

Whole-cell patch-clamp analysis of OSNs from the MOE *in situ* under conditions that largely suppress cation currents (**Fig. 5**) revealed Ca^{2+}-activated Cl^- currents (**Fig. 5d**,**f**,**g**,**i**) that were not observed in the absence of intracellular Ca^{2+} (**Fig. 5a**–**c**). These currents showed typical time-dependence and outward rectification at 1.5 µM (**Fig. 5d**,**f**), but not at 13 µM free Ca^{2+} (**Fig. 5g,i**) similar to data reported for Ca^{2+}-activated Cl^- currents for heterologously expressed Ano1 and Ano2[20-22,33,34] and for frog OSNs[7]. We could not detect these Cl^- currents in *Ano2*$^{-/-}$ OSNs (**Fig. 5e**,**f**,**h**,**i**). To exclude that transient Ca^{2+}-activated Cl^- currents remain in *Ano2*$^{-/-}$ OSNs, we used flash photolysis of caged Ca^{2+} and 8-Br-cAMP with isolated receptor neurons (**Fig. 6**). As observed previously[12,35], *Ano2*$^{+/+}$ neurons responded to uncaging of Ca^{2+} with large, rapidly activating, transient currents that reversed close to the Cl^- equilibrium potential (**Fig. 6a**,**c**). Currents in *Ano2*$^{-/-}$ OSNs were reduced to less than 10% of wild-type currents and reversed close to the K^+ equilibrium potential. Flash release of 8-Br-cAMP elicited large currents in *Ano2*$^{+/+}$ but not in *Ano2*$^{-/-}$ OSNs (**Fig. 6b**). Currents remaining in *Ano2*$^{-/-}$ neurons probably represent cation currents through CNG channels[12]. We conclude that Ca^{2+}-activated Cl^- currents of OSNs are mediated by Ano2.

In the VNO, both *Ano2*$^{+/+}$ and *Ano2*$^{-/-}$ VSNs had low background currents in the absence of intracellular Ca^{2+} (**Fig. 5j**–**l**). In *Ano2*$^{+/+}$ VSNs, 1.5 µM $[Ca^{2+}]_i$ elicited Cl^- currents with an outwardly rectifying, time-dependent component (**Fig. 5l**,**m**). Currents of most *Ano2*$^{-/-}$ VSNs were undistinguishable from those observed without Ca^{2+} (**Fig. 5n**), but a few cells showed currents up to twofold larger. Averaged current/voltage curves revealed that Ca^{2+}-activated Cl^- currents of VSNs depend predominantly on Ano2 (**Fig. 5l**). Although Ano1 is expressed in the VNO (**Fig. 3a**), its contribution to VSN currents seems minor.

Disruption of *Ano2* moderately reduces EOGs

We investigated the role of Ano2 in the MOE response to odorants using EOGs *ex vivo* (**Fig. 7**). In fluid-phase EOGs, we continuously superfused the surface of turbinates with Ringer solution and applied an odorant cocktail (**Fig. 7a**,**b**). The superfusate could be switched to a solution containing niflumic acid (NFA). NFA has been widely used to block Ca^{2+}-activated Cl^- channels in OSNs and other

cells[4,6,9,11,16,34,36,37] and inhibits both Ano1 and Ano2[18,20,21,33,34]. The response to odorants was reduced by roughly 40% in *Ano2*$^{-/-}$ EOGs compared to the wild type (**Fig. 7e**). We observed similar reductions in EOG amplitudes caused by *Ano2* disruption when adenylate cyclase was directly activated by forskolin (**Fig. 7c**–**e**), or with single odorants (**Fig. 7f**). As expected, NFA-insensitive voltage excursions were similar in both genotypes (**Fig. 7e**). Notably, NFA also inhibited odorant-induced responses in *Ano2*$^{-/-}$ epithelia (**Fig. 7b,e**). Comparison between *Ano2*$^{+/+}$ and *Ano2*$^{-/-}$ mice revealed that only ~60% of the response to NFA was due to an inhibition of Ano2. Hence, previous studies[9,11,37] may have overestimated the role of Ca^{2+}-activated Cl^- channels in olfaction.

In air-phase EOGs, we exposed the surfaces of turbinates to water-saturated air, and we applied an odorant or vehicle using an air puff. In this configuration, mucosal ion concentrations are expected to more closely match physiological levels. In cotnrast with our results for fluid-phase EOGs (**Fig. 7a**–**f**), we detected no significant differences between the genotypes in air phase (**Fig. 7g**).

With appropriate driving forces, apical Cl^- channels may change mucosal ion composition, similar to the proposed role of Ano1 in secretory epithelia[18,27,28]. However, Cl^--sensitive microelectrode measurements showed no difference in mucosal [Cl^-] between the genotypes (*Ano2*$^{+/+}$: 84.0 ± 11.8 mM (s.e.m., n = 6), *Ano2*$^{-/-}$: 84.4 ± 9 mM (s.e.m., n = 11)). These values agree with data from amphibia[15].

No olfactory deficits detected in *Ano2*$^{-/-}$ mice

Using an automated olfactometer[17,30,38,39], we tested the mice using an associative olfactory learning task. The mice were trained to sample two different stimuli, one of which was associated with a water reward, and to lick only in response to the rewarded odor.

Disruption of *Ano2* did not affect the mice's performance in discrimination tests in which they learned to distinguish geraniol from the mineral oil solvent (**Fig. 8a**). By contrast to *Ano2*$^{-/-}$ mice, *Cnga2*$^{-/y}$ mice[31] showed a clear-cut impairment in the same test (**Fig. 8a**), as reported[25,30]. Discrimination ability was neither reduced in more complex discrimination tasks such as distinguishing hexanal from octanal (**Fig. 8b**), or differentiating between (–)-limonene and an enantiomeric mixture of equal parts of (+)- and (–)-limonene (**Fig. 8c**). Discrimination between 0.4% hexanal/0.6% octanal and 0.6% hexanal/0.4% octanal was even more difficult, as evident from the larger number of trials needed to distinguish both mixtures (**Fig. 8d**). Even in this task, *Ano2*$^{-/-}$ mice performed similarly to wild type. Using successive dilutions of geraniol, we tested whether the loss of *Ano2* affected odor sensitivity. With either

genotype, odor detection dropped sharply when the dilution reached 10^{-7} (**Fig. 8e**). We conclude that Ca^{2+}-activated Cl^- channels are not essential for olfaction.

DISCUSSION

Ca^{2+}-activated Cl^- channels are prominently expressed in olfactory sensory neurons. In freshwater animals, in which ion gradients preclude a depolarizing influx of monovalent cations, Cl^- efflux may generate almost all of the receptor current[5,40]. By contrast, the cation concentration in the mucus surrounding olfactory cilia in mammals[14,15] allows for a sizeable depolarization when CNG channels open upon an odorant-induced rise in cAMP. After first publications had shown that Ca^{2+}-activated Cl^- currents could powerfully amplify olfactory receptor currents[4-7], this concept has received support from many groups. Experiments with isolated receptor neurons[4-6,8] showed that up to 80-90% of the receptor current is carried by Cl^-. An important role for Cl^- in olfaction was also inferred from EOGs[11,16,37]. However, as the molecular identity of the olfactory Ca^{2+}-activated Cl^- channel has remained elusive[35], the role of Cl^- channels in olfaction could not be tested directly.

Olfactory cilia express Bestrophin-2 (Best2; ref. 41) and Ano2 (refs. 13, 21), which were both hypothesized to mediate ciliary Ca^{2+}-activated Cl^- currents. A role of Bestrophin-2 has recently been excluded by normal Cl^- currents in *Best2*$^{-/-}$ OSNs[35]. The present work unambiguously identifies Ano2 as olfactory Ca^{2+}-activated Cl^- channel, or at least as an essential component thereof. Although Ano1 is expressed in the VNO, its contribution to Ca^{2+}-activated Cl^- currents in VSNs seems minor.

Unexpectedly, *Ano2*$^{-/-}$ mice had no detectable impairment of olfaction. This is not due to a compensatory upregulation of other Ca^{2+}-activated Cl^- channels or of the cyclic-nucleotide-gated channel. The normal growth and survival of newborn *Ano2*$^{-/-}$ mice already indicated that they could smell the teats of their mothers. Near-normal olfaction was suggested indirectly by unaltered tyrosine hydroxylase expression in the olfactory bulb and by apparently normal axonal coalescence on glomeruli in the olfactory bulb, and it was confirmed by quantitative olfactometry. In contrast to *Ano*$^{-/-}$ mice, *Cnga2*$^{-/y}$ mice have severely impaired olfaction (refs. 25,30 and present work). We conclude that CNG-mediated cation currents do not need an additional boost from anion currents for near-physiological levels of olfactory sensitivity.

Although fluid-phase EOGs revealed a significant difference between the genotypes, the ~40% reduction of *Ano2*$^{-/-}$ EOG amplitudes is much less than expected from the published 80-90% contribution of Cl^- to OSN receptor currents[8,11,12]. The contribution of Ca^{2+}-activated Cl^- channels was often estimated from the inhibition by NFA[11,37], but this compound also modulates several other ion

channels (for example, refs. 42,43). The attenuation of *Ano2*$^{-/-}$ EOGs by NFA now demonstrates that NFA also affects MOE targets other than Ca^{2+}-activated Cl^- channels. Hence, previous studies based on NFA-inhibition[11,37] have overestimated the role of Ca^{2+}-activated Cl^- channels. These channels might contribute only about 40% to receptor currents *in vivo*.

The ~40% reduction of fluid-phase EOG in *Ano2*$^{-/-}$ mice fits well to the ~39% to ~57% reduction of EOG amplitudes in *Nkcc1*$^{-/-}$ mice[11,16]. The $Na^+K^+2Cl^-$ co-transporter Nkcc1 may accumulate Cl^- into OSNs[9-11,13], a prerequisite for depolarizing Cl^- currents. On the basis of the NFA-block of *Nkcc1*$^{-/-}$ EOG responses, the authors[11] concluded that a substantial depolarizing Cl^- current remained in *Nkcc1*$^{-/-}$ OSNs and proposed that other transporters contribute to intracellular Cl^- accumulation[11,16]. The sizeable nonspecific component of NFA inhibition observed here, however, suggests that their results[11,16] are consistent with Nkcc1 being the main Cl^- accumulator of OSNs. In *Nkcc1*$^{-/-}$ mice, intraciliary [Cl^-] is then expected to be close to equilibrium, and opening of Ano2 channels should shunt rather than amplify receptor currents. Such a shunting inhibition may explain the larger decrease of EOG amplitudes in *Nkcc1*$^{-/-}$ mice compared to *Ano2*$^{-/-}$ mice.

How can the roughly 40% reduction of fluid-phase EOG amplitude, and almost no reduction of air-phase EOGs, be reconciled with previous studies that reported a large, up to 80-90% contribution of Cl^- to receptor currents? Many of those studies used isolated receptor neurons that were patch-clamped at the cell body[1,4-8,12]. Also, our experiments on isolated OSNs suggest a ~90% contribution of Ano2 to cAMP-induced currents. The disruption of tight junctions during isolation of OSNs may allow ciliary Ano2 channels to spread to the cell body where their electrical accessibility is much better[10]. The length (20–30 µm) and small diameter (0.1 µm) of cilia implies that channels in their distal part contribute little to voltage changes at the cell body, in particular when ciliary membrane conductance is high during signal transduction[44].

Another important consequence of ciliary geometry is the rapid dissipation of ion gradients. Taking into account ion concentrations measured in the mucus and the dendritic knob (as surrogate for cilia)[10,14,15], Cl^- gradients across the ciliary membrane should dissipate more easily than those for Na^+ or Ca^{2+} which carry depolarizing currents through CNG channels. Nkcc1 is thought to rapidly replenish ciliary Cl^-, which exits through anion channels during signal transduction[10,13]. Under physiological conditions, the driving force for Nkcc1-mediated ciliary Cl^- uptake is small[10] owing to rather low mucosal [Na^+] (55 or 85 mM[14,15]) and [Cl^-] (55 or 93 mM[14,15]; 84 mM (this work)). The driving force for Cl^- uptake is larger in extracellular

Ringer-type solutions (> 140 mM NaCl) that were used with isolated OSNs. Hence, more efficient ciliary Cl^- replenishment from Ringer solution than from mucus may lead to larger signal amplification by Cl^- channels in isolated OSNs and in fluid-phase EOGs than observed in air-phase EOGs and olfaction *in vivo*.

If the 40% reduction in *Ano2*$^{-/-}$ fluid-phase EOG amplitude translates into a similar reduction of action potential firing *in vivo*, our olfactory tests may not be sensitive enough to detect ensuing moderate changes in olfaction thresholds. On the other hand, air-phase EOGs, which more closely reflect the physiological situation, were not significantly impaired by *Ano2* disruption, suggesting that the olfactory information conveyed to the brain might be nearly unchanged. Notably, there are patients with van Willebrand syndrome who carry a large genomic deletion[45] that includes *ANO2* (*TMEM16B*). Consistent with the present work, no impairment of olfaction was reported. The expression of Ca^{2+}-activated Cl^- channels in mammalian OSNs may be an evolutionary vestige from freshwater animals[5,40], or it may serve also in mammals to allow consistent olfaction in face of variations of extracellular ion concentrations. Ano2 may also affect the mucosal fluid film in face of strong odors, although we showed unaltered mucosal Cl^- concentration under steady-state conditions. Alternatively, Ano2 might confer a slight increase in olfactory sensitivity that provides an evolutionary advantage. Clearly, however, Ca^{2+}-activated Cl^- channels are dispensable for near-normal olfaction, and the importance of these channels for olfactory signal amplification has been overestimated.

ACKNOWLEDGEMENTS

We thank P. Mombaerts (Max Planck Institute for Biophysics) for providing *Cnga2*$^{-}$, P2-IRES-tauLacZ and M72-IRES-tauLacZ mice, V. Hagen (FMP) for caged 8-Br-cAMP, I. Zarour and U. Heinemann (Charité) for help with ion-selective microelectrodes, S. Jabs and L. Leisle for help with flash photolysis, P. Mombaerts and B. Schroeder (MDC) for helpful discussions, and N. Krönke and F. Binder for technical assistance. This work was supported, in part, by the Prix Louis-Jeantet de Médecine to T.J.J.

AUTHOR CONTRIBUTIONS

G.M.B. generated *Ano2*$^{-/-}$ mice and Ano2 antibodies, designed, performed and evaluated expression analysis and immunohistochemistry, olfactometry and mouse behavioral studies and wrote the paper. B.P. designed, performed and evaluated patch-clamp analysis, EOG and ion-selective microelectrode measurements, and wrote the paper. B.P. and P.F. designed, performed and evaluated flash-photolysis experiments. T.J.J. initiated the project, designed and evaluated experiments and wrote the paper.

FIGURE LEGENDS

Figure 1 Immunoblot analysis of Ano2 expression. (**a**) Ano2 expression in the MOE, VNO and eye from *Ano2*$^{+/+}$, but not *Ano2*$^{-/-}$, mice. Protein loaded: 16 µg (MOE) and 100 µg (other lanes). (**b**) Ano2 is detected in lower amounts in the olfactory bulb, midbrain and brainstem, but not in the cortex, cerebellum and trigeminus. The loading control was α-tubulin. Protein loaded: MOE, 1.6 µg; eye, 10 µg; other lanes, 50 µg. The sharp ~140 kDa band remaining in *Ano2*$^{-/-}$ tissue is nonspecific. The broad band (*) in midbrain and brain stem tissue represents Ano2, as it is absent from *Ano2*$^{-/-}$ tissue and runs at a similar size as in the retina.

Figure 2 Ano2 localizes to sensory protrusions in olfactory epithelia. (**a**) Coronal view of the anterior part of the nasal cavity stained for Ano2 (antibody rbAno2_N3-3). Ano2 localized to the surface of the MOE and the VNO, but not to the respiratory epithelium (RE). Nuclei (blue) are shown only in the right half of the picture. Scale bar, 500 µm. (**b**) Confocal images of the transition region from MOE to respiratory epithelium shows Ano2 expression exclusively in OSNs, where it colocalizes with acetylated tubulin. (**c**) Colocalization of Ano2 and Cnga2 in the MOE. Merged images with nuclei labeled in blue are superimposed on transmission light pictures. Scale bar, 20 µm. Arrowheads mark transition from MOE to respiratory epithelium.

Figure 3 Ano2 and Ano1 are co-expressed in the VNO but not in the MOE. (**a**) A confocal image of the VNO colabeled for Ano2 (antibody gpAno2_C1-3) and Ano1 shows that both proteins are expressed in sensory protrusions of VSNs. Staining of *Ano2*$^{-/-}$ VNO confirms anti-Ano2 antibody specificity and reveals normal expression and localization of Ano1. Insets in merge, higher magnification of boxed areas. (**b**) Overview of nasal septum stained for Ano1. Arrowheads mark transition between MOE and respiratory epithelium (RE), and an asterisk marks the region containing nasal glands. (**c**,**d**) Ano1 expression is present only in non-ciliated cells of the respiratory epithelium that lack staining by the cilia marker acetylated tubulin (acTub) (highlighted in high-magnification insets in **c**). Beneath the respiratory epithelium, Ano1 is found in apical membranes of nasal gland epithelia (arrows and high-magnification inset in **d**). Nuclei are labeled in blue, and merged images are superimposed on transmission light pictures. Scale bars, 20 µm (**a**,**c**–**d**), 50 µm (**b**).

Figure 4 The olfactory bulb in *Ano2*$^{-/-}$ and *Ano2*$^{+/+}$ mice. (**a**) Specific staining for Ano2 in the olfactory nerve layer and in axons entering olfactory glomeruli. The section shows part of olfactory bulb from both hemispheres, with the cleft in center. Activity-dependent tyrosine hydroxylase (TH) expression in periglomerular cells is not changed in *Ano2*$^{-/-}$ section. (**b**) Higher magnification of a glomerulus stained for Ano2 and TH. Scale bars: 200 µm (**a**) and 50 µm (**b**). (**c**–**e**) Axonal coalescence of OSNs expressing the P2 (**c**,**d**) or M72 (**e**) olfactory receptors on glomeruli in the olfactory bulb. Olfactory bulbs of homozygous P2-IRES-tauLacZ or M72-IRES-tauLacZ mice[31] with disrupted or wild-type *Ano2* genes were stained for LacZ. Bulbi were sectioned (**c**), or the ventral (**d**) or dorsal (**e**) side of intact bulbi was observed. No difference in coalescence was seen (Number of mouse pairs: P2, *n* = 9 (4-15 weeks-old), M72, *n* = 2 (5 weeks-old) and *n* = 1 (24 weeks-old)). Scale bars, 0.5 mm (**c**), 1 mm (**d**,**e**).

Figure 5 Effect of *Ano2* disruption on Ca^{2+}-activated Cl^- currents. Patch-clamp recordings of olfactory receptor neurons from the MOE (**a**–**i**) and the VNO (**j**–**l**). (**a**,**d**,**g**) Typical current traces obtained from *Ano2*$^{+/+}$ OSNs in the presence of nominally 0 µM, 1.5 µM, and 13 µM Ca^{2+} in the recording pipette, respectively. The voltage-clamp protocol is shown in (**a**). (**b**,**e**,**h**) Current densities (*I*/*C*) from *Ano2*$^{-/-}$ OSNs under conditions as in **a**,**d**,**g**. (**c**,**f**,**i**) Averaged current-voltage relationships of steady-state currents with 0 µM, 1.5 µM and 13 µM Ca^{2+} in the pipette, respectively. ■, wild-type cells, Δ, *Ano2*$^{-/-}$ cells. Error bars, s.e.m. Number of cells measured: (**c**) 7 wild type, 7 knockout; (**f**), 15 wild type, 11 knockout; (**i**), 14 wild type, 10 knockout. (**j**,**m**) Typical current traces of wild-type vomeronasal sensory neurons (VSNs) with 0 µM Ca^{2+} (**j**) and 1.5 µM free Ca^{2+} (**m**) in the pipette. (**k**) *Ano2*$^{-/-}$ VSN with 0 µM Ca^{2+}, and (**n**) with 1.5 µM Ca^{2+} in the pipette. (**l**) Averaged current-voltage relationships from VNO receptor neurons measured with 1.5 µM Ca^{2+} (■ *Ano2*$^{+/+}$, □ *Ano2*$^{-/-}$; *n* = 7 and 6, respectively) and with 0 µM Ca^{2+} (● wild type, ○ *Ano2*$^{-/-}$; *n* = 5 for both). Error bars, s.e.m. Voltage clamp protocol as in **a**.

Figure 6 Response of isolated olfactory receptor neurons to photoreleased Ca^{2+} or 8-Br-cAMP. (**a**) Typical current responses to sudden [Ca^{2+}] increase of isolated OSNs from both genotypes in whole-cell patch-clamp experiments under symmetrical Cl^-. Cells were clamped to -50 mV, 0 mV and +50 mV. Arrows indicate the flash that releases Ca^{2+} from DMNP-EDTA. *Inset*, larger magnification to reveal the currents remaining in *Ano2*$^{-/-}$ OSNs. (**b**) Typical currents elicited by flash release of 8-Br-cAMP (arrows) in isolated OSNs from *Ano2*$^{+/+}$ and *Ano2*$^{-/-}$ mice held at -50 mV. Mean amplitudes were -445 ± 111 pA and -43.2 ± 9.9 pA for *Ano2*$^{+/+}$ and *Ano2*$^{-/-}$ OSNs, respectively (±s.e.m., p = 0.0016). (**c**) Peak currents elicited by uncaging Ca^{2+} as function of holding voltage, averaged from eight *Ano2*$^{+/+}$ and seven *Ano2*$^{-/-}$ OSNs with three or more mice per genotype. Error bars, s.e.m. Significance levels (two sample *t*-test): *, $P < 0.05$; **, $P < 0.01$.

Figure 7 EOGs from the MOE. (**a,b**) Typical fluid phase EOGs from *Ano2*$^{+/+}$ (**a**) from *Ano2*$^{-/-}$ (**b**) mice with a mixture of 17 odorants ('Mix1': isopentyl acetate, hexanal, eucalyptol, limonene, 2-heptanone, menthyl acetate, peppermint oil, eugenol, ethyl valerate, ethyl butyrate, ethyl tiglate, allyl tiglate, octanal, isobutyl propionate, acetal, hexanoic acid, 2-hexanene, 100 µM each). Bars above traces indicate application (200 ms) of odorant mixture (lower trace) or vehicle (upper trace). Grey traces were obtained with 300 µM NFA and black traces in Normal Ringer (NR) before and after exposure to NFA (washout). Traces were averaged from responses to ten repeated stimuli. (**c**,**d**) Typical fluid-phase EOGs evoked by 2-s application of 30 µM forskolin (lower trace) or vehicle control (upper trace) to *Ano2*$^{+/+}$ (**c**) and *Ano2*$^{-/-}$ MOE (**d**). (**e**) Averaged EOG amplitudes from experiments as in **a**–**d**. (**f**) Averaged fluid-phase EOG amplitudes elicited by individual odorants at 1 mM concentration and with 1:20 diluted coyote urine. (**g**) Averaged air phase EOG amplitudes from mice of both genotypes. 'Mix1' is the same odorant mixture as in **a**. 'Mix2' contained eight odorants (D-carvone, 1-heptanol, 2-methylbutyric acid, geraniol, isopentylamine, 2-hexanone, acetophenone, 1-octanal). Differences in responses between genotypes are not statistically significant. Numbers in columns, number of measurements; error bars, s.e.m. Significance levels (two sample *t*-test): *, $P < 0.05$; **, $P < 0.01$; ***, $P < 0.001$.

Figure 8 *Ano2* disruption affected neither odor discrimination nor olfactory sensitivity. (**a**–**d**) Different discrimination tasks. As true for wildt-type littermates, *Ano2*$^{-/-}$ mice learned to discriminate between 1% geraniol and the diluent mineral oil (*n* = 6 for each genotype) (**a**), between 1% hexanal and 1% octanal (*n* = 3 for each genotype) (**b**), between 1% (–)-limonene and an enantiomeric mixture of 0.5% (–)-limonene and 0.5% (+)-limonene (*n* = 4 for each genotype) (**c**), and between 0.4%hexanal/0.6%octanal and 0.6%hexanal/0.4%octanal (*n* = 5 for each genotype) (**d**). Anosmic *Cnga2*$^{-/y}$ mice (*n* = 3) could not detect 1% geraniol (**a**). (**e**) Odor detection threshold for geraniol. Both *Ano2*$^{-/-}$ (*n* = 6) and *Ano2*$^{+/+}$ littermates (*n* = 6) detected geraniol and discriminated it from the diluent only down to a dilution of 10^{-6}. The first data point with a geraniol dilution of 10^{-2} corresponds to **a**. Error bars, s.e.m. There was no significant difference between *Ano2*$^{+/+}$ and *Ano2*$^{-/-}$ mice in any of these tests.

ONLINE METHODS

***Ano2*$^{-/-}$ mice.** An 11 kb genomic region of *Ano2* spanning exon 12 and 13 was cloned from R1 ES cells by PCR. Exon 12 was flanked with loxP sites, a FRT-flanked neomycin selection cassette inserted (**Supplementary Fig. 1**) and the construct cloned into pKO Scrambler plasmid 901 (Lexicon Genetics). The linearized targeting vector was electroporated into R1 ES cells (129/SvJ). Cells from two independent correctly targeted clones were injected into C57BL/6 blastocysts. Chimeras were crossed to C57BL/6 Cre *deleter* mice[24] for *in vivo* excision of exon 12, which eliminates part of the first extracellular loop and of the second transmembrane domain. Splicing from exon 11 to exon 13 introduces a frameshift after the first transmembrane domain. Mice were in a mixed C57BL/6-129/Svj background and littermates served as controls. The mice in experiments were older than 4 weeks. We carried out genotyping PCR with primers flanking the loxP site of the *Ano2*$^{-}$ allele (5'-GGACACCCCGTACTTGAAGA-3' and 5'-AGCACAATGCAGACCAAGTT-3'), yielding 163-bp and 1051-bp products for Ano^{-} and Ano^{+} alleles, respectively.

Mouse husbandry. Animal care and experiments conformed to German animal protection laws and were approved by the Berlin authorities (LaGeSo). *Cnga2*$^{-}$ (previously called *Ocnc1*$^{-}$), P2-IRES-tauLacZ and M72-IRES-tauLacZ mice were provided by P. Mombaerts (Max Planck Institute of Biophysics, Frankfurt) and have been described[31].

Generation of Ano2 antibodies. Antibody to the the N-terminal epitope (^{128}NGETGKERHGGGPGDVELG) of Ano2 (rbAno2_N3-3) was raised in rabbits; antibody to the extreme C-terminus (^{970}GDRSRRSRAASSAPSGRSQP) of Ano2 (gpAno2_C1-3) was raised in guinea pigs (Pineda Antikörper-Service, Berlin). Peptides were coupled to keyhole limpet hemocyanine via C- and N-terminally added cysteines, respectively. The animals were immunized seven times, and the antibodies were affinity-purified from final bleeds and tested using *Ano2*$^{-/-}$ tissue as control.

Immunohistochemistry. Anesthetized mice were perfused with PBS followed by 4% paraformaldehyde (PFA) (wt/vol) in PBS. Tissues were post-fixed for 2 h (olfactory bulb) or overnight (nose, eye). We cut 6-µm cryosections from the eye and 10-µm cryosections from olfactory bulb. Noses were decalcified in 10% EDTA (wt/vol) in PBS for 7 d and post-fixed for 2 h, and then 6-µm paraffin sections were prepared.

For antigen retrieval, sections were boiled for 5 min in 10 mM citrate buffer (pH 6.0) or 10 mM Tris, 1 mM EDTA (pH 9.0), and transferred to 3% BSA (wt/vol) in TBS with 0.2% NP-40 (vol/vol) for blocking and antibody incubation. Antibodies were used at the following dilutions: rbAno2_N3-3 (1:1000); gpAno2_C1-3 (1:250); anti-TMEM16A (Ano1) rabbit polyclonal (1:100, ab53212, Abcam; its specificity had been shown using *Ano1*$^{-/-}$ tissue[46]); anti-Cnga2 goat polyclonal (1:50, CNG-2/M-20, sc-13700, Santa Cruz); anti-acetylated tubulin mouse monoclonal (1:1000, clone 6-11B-1, T7451, Sigma-Aldrich); anti-tyrosine hydroxylase mouse monoclonal (1:1000, MAB5280, Chemicon); anti–PSD-95 mouse monoclonal (1:250, clone 7E3-1B8, MA1-046, ThermoScientific); anti-PMCA mouse monoclonal (1:500, clone 5F10, MA3-914, Affinity BioReagents). Detection was carried out using secondary antibodies coupled to Alexa fluorophores (Invitrogen). Nuclei were stained with Hoechst 33258. Pictures were taken with a Zeiss LSM 510 META laser scanning microscope using a Plan-Apochromat 63×/1.40 Oil DIC M27 or EC Plan-Neofluar 10×/0.3 M27 objective and ZEN software.

Determination of OSN coalescence. P2-IRES-tauLacZ and M72-IRES-tauLacZ mice[31] were crossed with *Ano2*$^{+/-}$ mice to yield *Ano2*$^{-/-}$ and *Ano2*$^{+/+}$ littermates that were homozygous for these reporter lines. Experiments were carried out with mice from 5 weeks to 24 weeks old. The mice were perfused with PBS followed by 4% PFA (wt/vol) in PBS. Brains were post-fixed (20 min on ice), washed in buffer A (100 mM phosphate buffer (pH 7.4), 2 mM $MgCl_2$, 5 mM EGTA) and incubated for 30 min in buffer A with 0.02% NP-40 (vol/vol) and 0.01% deoxycholate (vol/vol). LacZ staining was overnight in buffer A with 0.2% NP-40 (vol/vol), 0.1% deoxycholate (vol/vol), 5 mM potassium-ferricyanide, 5 mM potassium-ferrocyanide and 1 mg ml^{-1} of X-Gal at room temperature (20-25℃). Whole-mount stained bulbs were cryoprotected in 30% sucrose (wt/vol), frozen in Tissue-Tek O.C.T. compound (Sakura) and cut into 20-µm cryostat sections. Sections were post-stained with X-Gal and counterstained with Neutral Red.

Lysate preparation, deglycosylation and immunoblotting. Turbinates, VNO or eyes were dissected, minced and sonicated in lysis buffer (10 mM HEPES (pH 7.4), 150 mM NaCl, 5 mM EDTA, protease inhibitors, 1% SDS (wt/vol)). Lysates from brain regions and ANO1-transfected HEK cells were prepared similarly. The ANO1 expression construct encodes a 986 aa human isoform (NM_018043.5). For deglycosylation, lysates were incubated with 5% β-mercaptoethanol (vol/vol) for 15

min at 55 °C, diluted 1:5 into deglycosylation buffer (50 mM HEPES (pH 7.4), 10 mM EDTA, 0.5% Nonidet P-40 (vol/vol) and protease inhibitors) and incubated overnight at 37 °C with 1 U of N-Glycosidase F (Roche Diagnostics) per 100 µg protein. Proteins were separated on SDS-polyacrylamide gels and transferred on polyvinylidene difluoride membranes. Antibodies were used at the following dilutions: rbAno2_N3-3 antibody (1:1000); anti-adenylate cyclase III rabbit polyclonal (1:2000, C-20, sc-588, Santa Cruz); anti-olfactory marker protein (OMP) goat polyclonal (1:1000, 544-10001, Wako); anti-α-tubulin mouse monoclonal (1:2000, clone B-5-1-2, T5168, Sigma-Aldrich); anti-Cnga2 (1:100), anti-tyrosine hydroxylase (1:5000) and anti-TMEM16A (1:250) antibodies as in immunohistochemistry. Signals were visualized by chemiluminescence (SuperSignal West, Pierce) with a PeqLab camera system and secondary antibodies coupled to horseradish peroxidase (Chemicon). Immunoblots were repeated in three or more independent experiments.

Quantitative real-time PCR. Turbinates were dissected from *Ano2*$^{+/+}$ and *Ano2*$^{-/-}$ mice (three litter pairs, 25-27 weeks old) and total RNA was isolated (RNeasy Mini Kit, Qiagen). We subjected 1 µg RNA to DNase I (amplification grade, Invitrogen) digestion and transcribed it into cDNA using random primers and Superscript II reverse transcriptase (Invitrogen). We set up 20-µl PCR reactions were set up with the Power SYBR Green PCR Master Mix (Applied Biosystems) and run the reactions in triplicates with 40-s elongation time at 60 °C. Amplification and melting curves were monitored using a StepOnePlus Real-Time PCR System and StepOne Software (Applied Biosystems). Comparison between *Ano2*$^{-/-}$ and wild-type littermates used the Pfaffl method and β-actin as internal control. Primers spanned introns or exon-exon boundaries and gave products of 100 to 200 bp length. Primer pairs: β-actin 5'-TGTGATGGTGGGAATGGGTCAGAA-3', 5'-TGTGGTGCCAGATCTTCTCCATGT-3'; adenylate cyclase III 5'-CGGCATCGAGTGTCTACGCTTC-3', 5'-GCCAGCGCTCCTTGTCTGACTT-3'; Ano2_ex3-4 5'-GATGTTGAACTTGGGCCACT-3', 5'-CAAGAACTCTGCTTCCCTGG-3'; Ano2_ex20-21 5'-AGGCTGTCTCATGGAGCTGT-3', 5'-TGCTCTGGACGTTTTGAGTG-3'; Ano6 5'-AAGAGGAACAGGCCCGGCCA-3', 5'-AGAAGACGGCGCTCGCACAC-3'; Ano8 5'-GCGACGCGGCTGGAAGACAG-3', 5'-CGGCCAGTGGGAAGGCAGAG-3'; Ano10 5'-AGCGGAAGTACTGTGCGAGGGT-3', 5'-GCAAAGGCAGCTGCTAGCGG-3'; Nkcc1 5'-CTGGTGGGCTGCGTTGCTCA-3', 5'-GCGCTTGTGTGGAGGATCCCC-3'.

Tissue preparation for patch-clamping. Mice were killed at 6-8 weeks by cervical dislocation. The MOE was prepared and embedded in 4% low melting agarose (wt/vol) in normal Ringer (140 mM NaCl, 5 mM KCl, 10 mM glucose, 1 mM sodium pyruvate, 10 mM HEPES (pH 7.4), 2 mM $CaCl_2$, 1 mM $MgCl_2$, osmolality: 321 mOsm kg^{-1}). A Leica VT1200S vibratome was used to cut 200-µm perpendicular to the surface. The soft tissue of the VNO was embedded[47] in 4% low melting agarose (wt/vol), and cut in 200-µm coronal slices. Slices were kept in normal Ringer bubbled with 95% O_2/ 5% CO_2.

Preparation of isolated olfactory receptor neurons. The MOE was transferred to low-Ca^{2+} Ringer (140 mM NaCl, 5 mM KCl, 10 mM glucose, 1 mM sodium pyruvate, 1 mM EDTA, 1 mM cysteine, 10 mM HEPES (pH 7.2)) at 4 °C. After mincing, it was digested at room temperature for 20 minutes with 0.2 mg ml^{-1} trypsin in low-Ca^{2+} Ringer. The digestion was terminated with normal Ringer containing 0.2 mg ml^{-1} BSA, 0.2 mg ml^{-1} leupeptin and 0.025 mg ml^{-1} DNase I. Following gentle trituration, cells were allowed to settle on poly-L-lysine–coated coverslips for 30-45 minutes at 4 °C.

Patch-clamp analysis. Pipettes were pulled from borosilicate glass and contained 140 mM CsCl, 4 mM HEPES (pH 7.2), 1 mM EGTA, 2 mM Mg-ATP. Free [Ca^{2+}] was adjusted according to the Maxchelator program (http://maxchelator.stanford.edu/) to 0 µM, 1.5 µM and 13 µM. OSNs from the MOE were patched at the cell body and sometimes at the dendritic knob, with similar results. VSNs were patch-clamped at the dendritic knob. Pipette resistances were ~ 5 MΩ and 8-10 MΩ when patching OSNs or VSN dendritic knobs, respectively. Recordings were performed in the whole-cell configuration at room temperature in normal Ringer containing 10 mM tetraethylammonium chloride using an Axon CNS MultiClamp 700B amplifier, a Digidata 1322A interface, and pClamp 10 software (Molecular Devices).

Photorelease of caged Ca^{2+} and 8-Br-cAMP. We used [6,7-Bis(carboxymethoxy)coumarin-4-yl]methyl-8-bromoadenosine-3', 5'-cyclic mono-phosphate (BCMCM-caged 8-Br-cAMP), a generous gift from V. Hagen (FMP, Berlin) and DMNP-EDTA (Invitrogen). For uncaging 8-Br-cAMP, a UV flash lamp JML-C2 (Rapp OptoElektronik) was coupled to an inverted Zeiss Axiovert 200 microscope equipped with a 100× Fluar objective. Ca^{2+} was uncaged with a SP-20 UV flash lamp (Rapp OptoElektronik) coupled to an upright Olympus BX51WI microscope equipped

with a 60× LUMPlanFL objective. Isolated OSNs were patched at room temperature in the whole-cell mode. For Ca^{2+} uncaging, the pipette solution contained 140 mM KCl, 2 mM MgATP, 0.3 mM Na_2-GTP, 10 mM HEPES (pH 7.4), 3.5 mM $CaCl_2$ and 5 mM DMNP-EDTA. For uncaging 8-Br-cAMP, the pipette solution contained 145 mM KCl, 4 mM $MgCl_2$, 1 mM MgATP, 0.1 mM Na_2-GTP, 10 mM HEPES (pH 7.4), 0.5 mM EGTA, and 0.1 mM BCMCM-caged 8-Br-cAMP. Settings were 200 V at 1 mF and 300 V at 3 mF for uncaging 8-Br-cAMP and Ca^{2+}, respectively.

Electro-olfactogram recordings. The head was cut in the sagittal plane and the endoturbinates were exposed[11,48]. The lateral side of the head was immersed into 0.5% agarose gel with Normal Ringer.

In fluid-phase EOGs the turbinates were continuously superfused with normal Ringer with or without niflumic acid. The four-barrelled application pipette had two channels for continuous flow of normal Ringer, a channel for odorant-free vehicle and for odorants. The latter two channels were connected to a Picospritzer (Toohey) to apply pressure steps. Mixtures of odorants, single odorant or forskolin (specified in legend to Fig. 7, in aqueous solution containing 0.5% DMSO (vol/vol)) were used.

In the air-phase configuration, the application tube had a channel for continuous flow of humidified 95% O_2/5% CO_2, and another one connected to a 15-ml bottle containing 2 ml of odorants or odorant-free vehicle, and a Picospritzer. Pressure steps of 200 ms were used to drive the air from the bottle to the turbinates. In both arrangements, EOGs were recorded in current clamp with an extracellular electrode filled with Ringer placed on the middle of turbinate IIb or III. EOG amplitudes from single turbinates were averaged from ten individual sweeps and subsequently averaged from several experiments.

Ion-sensitive microelectrodes. Chloride-selective electrodes were fabricated[49] from theta-glass capillaries (Warner Instruments) with tip diameters of ~3 µm. Ion-selective barrels were silanized with methyltrichlorosilane in dichloromethane (Fluka/Sigma-Aldrich) and backfilled with 'Chloride ionophore I – cocktail A' (Fluka/Sigma-Aldrich). Reference barrels contained 155 mM NaCl. To exclude artifacts by Cl^- diffusion, we also filled them with 40 mM NaCl and 77 mM Na_2SO_4. No differences in measured [Cl^-] were found. Measurements with either reference barrel solution were pooled. Microelectrodes connected to a differential amplifier[49] were lowered at a low angle onto the surface of freshly dissected turbinates. [Cl^-] was determined from calibration

curves before and after measurements. Measurements were discarded when these calibrations differed by >20%.

Olfactometry. Behavioral assessment of odor detection and discrimination ability used a computer-controlled 8-channel liquid-dilution olfactometer (Knosys) as described[50]. Mice were trained on a go/no-go operant conditioning task in which licking on a water delivery tube upon presentation of an S+ stimulus (odor 1) is associated with a water reward, but not after presentation of an S– stimulus (odor 2 or diluent). Mice able to discriminate between stimuli readily stop to answer to the S– stimulus when subjected to successive trials of S+ and S– stimuli presented in random order. Response accuracy is monitored as a measure for odor discrimination and detection ability and represents the percentage of correct answers in a block of 20 trials.

Water-deprived *Ano2*$^{-/-}$ mice and control littermates were trained on the BEGIN program and on a simple odor discrimination task. Tests used the D2 program with standard settings[50]. Chemicals were from Sigma-Aldrich/Fluka. Mice (35-41 weeks-old) were tested on 1% (–)-limonene versus 0.5% (–)/0.5% (+)-limonene (six males, two females) and on geraniol dilutions (eight males, four females) starting with the highest concentration. Trials were 200 (down to 10^{-5}) or 400 (10^{-6}, 10^{-7}) and response accuracy was calculated as mean of three consecutive blocks after reaching the criterion response of 90% or of the last three blocks in 400 trials, respectively. Mice at 14 weeks old (four males, two females) were used for 1% hexanal versus 1% octanal discrimination, and six males and fopur females (at 50 weeks old) for the 0.4/0.6% versus 0.6/0.4% hexanal/octanal discrimination test. Three male *Cnga2*$^{-/y}$ mice (14-16 weeks old) were tested on 1% geraniol.

REFERENCES

1. Kleene, S. J. The electrochemical basis of odor transduction in vertebrate olfactory cilia. *Chemical senses* **33**, 839-859 (2008).
2. Munger, S. D., Leinders-Zufall, T. & Zufall, F. Subsystem organization of the mammalian sense of smell. *Annu Rev Physiol* **71**, 115-140 (2009).
3. Bönigk, W. *et al.* The native rat olfactory cyclic nucleotide-gated channel is composed of three distinct subunits. *J Neurosci* **19**, 5332-5347 (1999).
4. Kleene, S. J. Origin of the chloride current in olfactory transduction. *Neuron* **11**, 123-132 (1993).
5. Kurahashi, T. & Yau, K. W. Co-existence of cationic and chloride components in odorant-induced current of vertebrate olfactory receptor cells. *Nature* **363**, 71-74 (1993).
6. Lowe, G. & Gold, G. H. Nonlinear amplification by calcium-dependent chloride channels in olfactory receptor cells. *Nature* **366**, 283-286 (1993).
7. Kleene, S. J. & Gesteland, R. C. Calcium-activated chloride conductance in frog olfactory cilia. *J Neurosci* **11**, 3624-3629 (1991).
8. Reisert, J., Bauer, P. J., Yau, K. W. & Frings, S. The Ca^{2+}-activated Cl channel and its control in rat olfactory receptor neurons. *J Gen Physiol* **122**, 349-363 (2003).
9. Reisert, J., Lai, J., Yau, K. W. & Bradley, J. Mechanism of the excitatory Cl^- response in mouse olfactory receptor neurons. *Neuron* **45**, 553-561 (2005).
10. Kaneko, H., Putzier, I., Frings, S., Kaupp, U. B. & Gensch, T. Chloride accumulation in mammalian olfactory sensory neurons. *J Neurosci* **24**, 7931-7938 (2004).
11. Nickell, W. T., Kleene, N. K., Gesteland, R. C. & Kleene, S. J. Neuronal chloride accumulation in olfactory epithelium of mice lacking NKCC1. *J Neurophysiol* **95**, 2003-2006 (2006).
12. Boccaccio, A. & Menini, A. Temporal development of cyclic nucleotide-gated and Ca^{2+}-activated Cl^- currents in isolated mouse olfactory sensory neurons. *J Neurophysiol* **98**, 153-160 (2007).
13. Hengl, T. *et al.* Molecular components of signal amplification in olfactory sensory cilia. *Proc Natl Acad Sci U S A* **107**, 6052-6057 (2010).
14. Reuter, D., Zierold, K., Schröder, W. H. & Frings, S. A depolarizing chloride current contributes to chemoelectrical transduction in olfactory sensory neurons in situ. *J Neurosci* **18**, 6623-6630 (1998).
15. Chiu, D., Nakamura, T. & Gold, G. H. Ionic composition of toad olfactory mucus measured with ion selective microelectrodes (Abstract). *Chemical senses* **13**, 677-678 (1988).
16. Nickell, W. T., Kleene, N. K. & Kleene, S. J. Mechanisms of neuronal chloride accumulation in intact mouse olfactory epithelium. *J Physiol* **583**, 1005-1020 (2007).
17. Smith, D. W., Thach, S., Marshall, E. L., Mendoza, M. G. & Kleene, S. J. Mice lacking NKCC1 have normal olfactory sensitivity. *Physiology & behavior* **93**, 44-49 (2008).
18. Yang, Y. D. *et al.* TMEM16A confers receptor-activated calcium-dependent chloride conductance. *Nature* **455**, 1210-1215 (2008).
19. Caputo, A. *et al.* TMEM16A, a membrane protein associated with calcium-dependent chloride channel activity. *Science* **322**, 590-594 (2008).
20. Schroeder, B. C., Cheng, T., Jan, Y. N. & Jan, L. Y. Expression cloning of TMEM16A as a calcium-activated chloride channel subunit. *Cell* **134**, 1019-1029 (2008).

21. Stephan, A. B. *et al.* ANO2 is the cilial calcium-activated chloride channel that may mediate olfactory amplification. *Proc Natl Acad Sci U S A* **106**, 11776-11781 (2009).
22. Stöhr, H. *et al.* TMEM16B, a novel protein with calcium-dependent chloride channel activity, associates with a presynaptic protein complex in photoreceptor terminals. *J Neurosci* **29**, 6809-6818 (2009).
23. Rasche, S. *et al.* Tmem16b is specifically expressed in the cilia of olfactory sensory neurons. *Chemical senses* **35**, 239-245 (2010).
24. Schwenk, F., Baron, U. & Rajewsky, K. A cre-transgenic mouse strain for the ubiquitous deletion of *loxP*-flanked gene segments including deletion in germ cells. *Nucleic Acids Res* **23**, 5080-5081 (1995).
25. Brunet, L. J., Gold, G. H. & Ngai, J. General anosmia caused by a targeted disruption of the mouse olfactory cyclic nucleotide-gated cation channel. *Neuron* **17**, 681-693 (1996).
26. Nakamura, T. & Gold, G. H. A cyclic nucleotide-gated conductance in olfactory receptor cilia. *Nature* **325**, 442-444 (1987).
27. Romanenko, V. G. *et al.* Tmem16A encodes the Ca^{2+}-activated Cl^- channel in mouse submandibular salivary gland acinar cells. *J Biol Chem* **285**, 12990-13001 (2010).
28. Rock, J. R. *et al.* Transmembrane protein 16A (TMEM16A) is a Ca^{2+}-regulated Cl^- secretory channel in mouse airways. *J Biol Chem* **284**, 14875-14880 (2009).
29. Keller, A. & Margolis, F. L. Immunological studies of the rat olfactory marker protein. *J Neurochem* **24**, 1101-1106 (1975).
30. Lin, W., Arellano, J., Slotnick, B. & Restrepo, D. Odors detected by mice deficient in cyclic nucleotide-gated channel subunit A2 stimulate the main olfactory system. *J Neurosci* **24**, 3703-3710 (2004).
31. Zheng, C., Feinstein, P., Bozza, T., Rodriguez, I. & Mombaerts, P. Peripheral olfactory projections are differentially affected in mice deficient in a cyclic nucleotide-gated channel subunit. *Neuron* **26**, 81-91 (2000).
32. Zou, D. J. *et al.* Absence of adenylyl cyclase 3 perturbs peripheral olfactory projections in mice. *J Neurosci* **27**, 6675-6683 (2007).
33. Pifferi, S., Dibattista, M. & Menini, A. TMEM16B induces chloride currents activated by calcium in mammalian cells. *Pflügers Arch* **458**, 1023-1038 (2009).
34. Sagheddu, C. *et al.* Calcium concentration jumps reveal dynamic ion selectivity of calcium-activated chloride currents in mouse olfactory sensory neurons and TMEM16B/anoctamin2-transfected HEK 293T cells. *J Physiol* **588**, 4189-4204 (2010).
35. Pifferi, S. *et al.* Calcium-activated chloride currents in olfactory sensory neurons from mice lacking bestrophin-2. *J Physiol* **587**, 4265-4279 (2009).
36. Frings, S., Reuter, D. & Kleene, S. J. Neuronal Ca^{2+} -activated Cl^- channels--homing in on an elusive channel species. *Prog Neurobiol* **60**, 247-289 (2000).
37. Pinato, G. *et al.* Electroolfactogram responses from organotypic cultures of the olfactory epithelium from postnatal mice. *Chemical senses* **33**, 397-404 (2008).
38. Bodyak, N. & Slotnick, B. Performance of mice in an automated olfactometer: odor detection, discrimination and odor memory. *Chemical senses* **24**, 637-645 (1999).
39. Kelliher, K. R., Ziesmann, J., Munger, S. D., Reed, R. R. & Zufall, F. Importance of the CNGA4 channel gene for odor discrimination and adaptation in behaving mice. *Proc Natl Acad Sci U S A* **100**, 4299-4304 (2003).

40. Kleene, S. J. & Pun, R. Y. Persistence of the olfactory receptor current in a wide variety of extracellular environments. *J Neurophysiol* **75**, 1386-1391 (1996).
41. Pifferi, S. *et al.* Bestrophin-2 is a candidate calcium-activated chloride channel involved in olfactory transduction. *Proc Natl Acad Sci U S A* **103**, 12929-12934 (2006).
42. Gribkoff, V. K. *et al.* Effects of channel modulators on cloned large-conductance calcium-activated potassium channels. *Mol Pharmacol* **50**, 206-217 (1996).
43. Vogalis, F., Hegg, C. C. & Lucero, M. T. Ionic conductances in sustentacular cells of the mouse olfactory epithelium. *J Physiol* **562**, 785-799 (2005).
44. Lindemann, B. Predicted profiles of ion concentrations in olfactory cilia in the steady state. *Biophys J* **80**, 1712-1721 (2001).
45. Schneppenheim, R. *et al.* A common 253-kb deletion involving *VWF* and *TMEM16B* in German and Italian patients with severe von Willebrand disease type 3. *J Thromb Haemost* **5**, 722-728 (2007).
46. Gomez-Pinilla, P. J. *et al.* Ano1 is a selective marker of interstitial cells of Cajal in the human and mouse gastrointestinal tract. *Am J Physiol Gastrointest Liver Physiol* **296**, G1370-1381 (2009).
47. Shimazaki, R. *et al.* Electrophysiological properties and modeling of murine vomeronasal sensory neurons in acute slice preparations. *Chemical senses* **31**, 425-435 (2006).
48. Cygnar, K. D., Stephan, A. B. & Zhao, H. Analyzing responses of mouse olfactory sensory neurons using the air-phase electroolfactogram recording. *J Vis Exp* (2010).
49. Windmüller, O. *et al.* Ion changes in spreading ischaemia induce rat middle cerebral artery constriction in the absence of NO. *Brain* **128**, 2042-2051 (2005).
50. Slotnick, B. & Restrepo, D. Olfactometry with mice. in *Current protocols in Neuroscience (eds. Crawley, J. N, et al.)* **Chapter 8**, Unit 8 20 (2005).

Figure 1

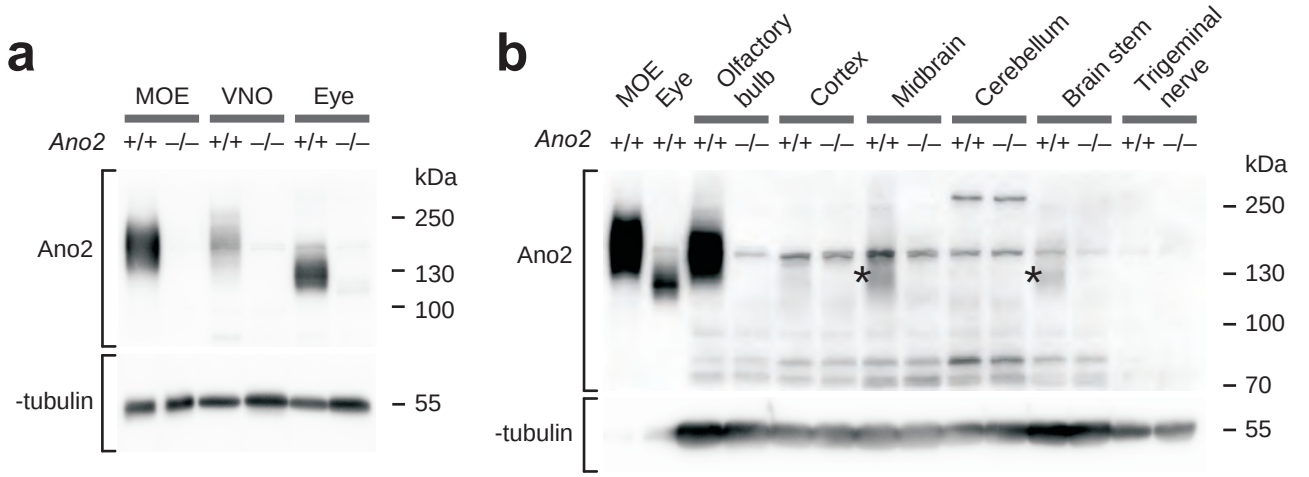
a
MOE
VNO
Eye
Ano2
+/+ –/– +/+ –/– +/+ –/–
kDa
Ano2
250
130
100
-tubulin
55
b
MOE
Eye
Olfactory bulb
Cortex
Midbrain
Cerebellum
Brain stem
Trigeminal nerve
Ano2
+/+ +/+ +/+ –/– +/+ –/– +/+ –/– +/+ –/– +/+ –/– +/+ –/–
kDa
Ano2
250
130
100
70
-tubulin
55
*
*

Figure 2

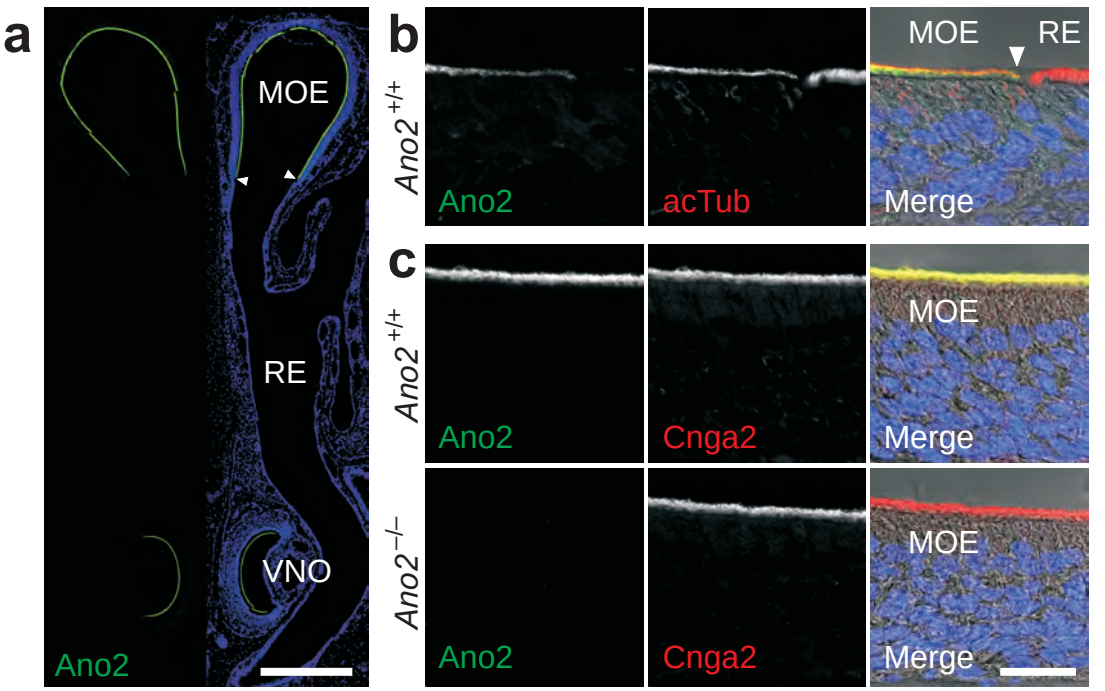
a
MOE
RE
VNO
Ano2
b
Ano2+/+
Ano2
acTub
MOE
RE
Merge
c
Ano2+/+
Ano2
Cnga2
MOE
Merge
Ano2−/−
Ano2
Cnga2
MOE
Merge

Figure 3

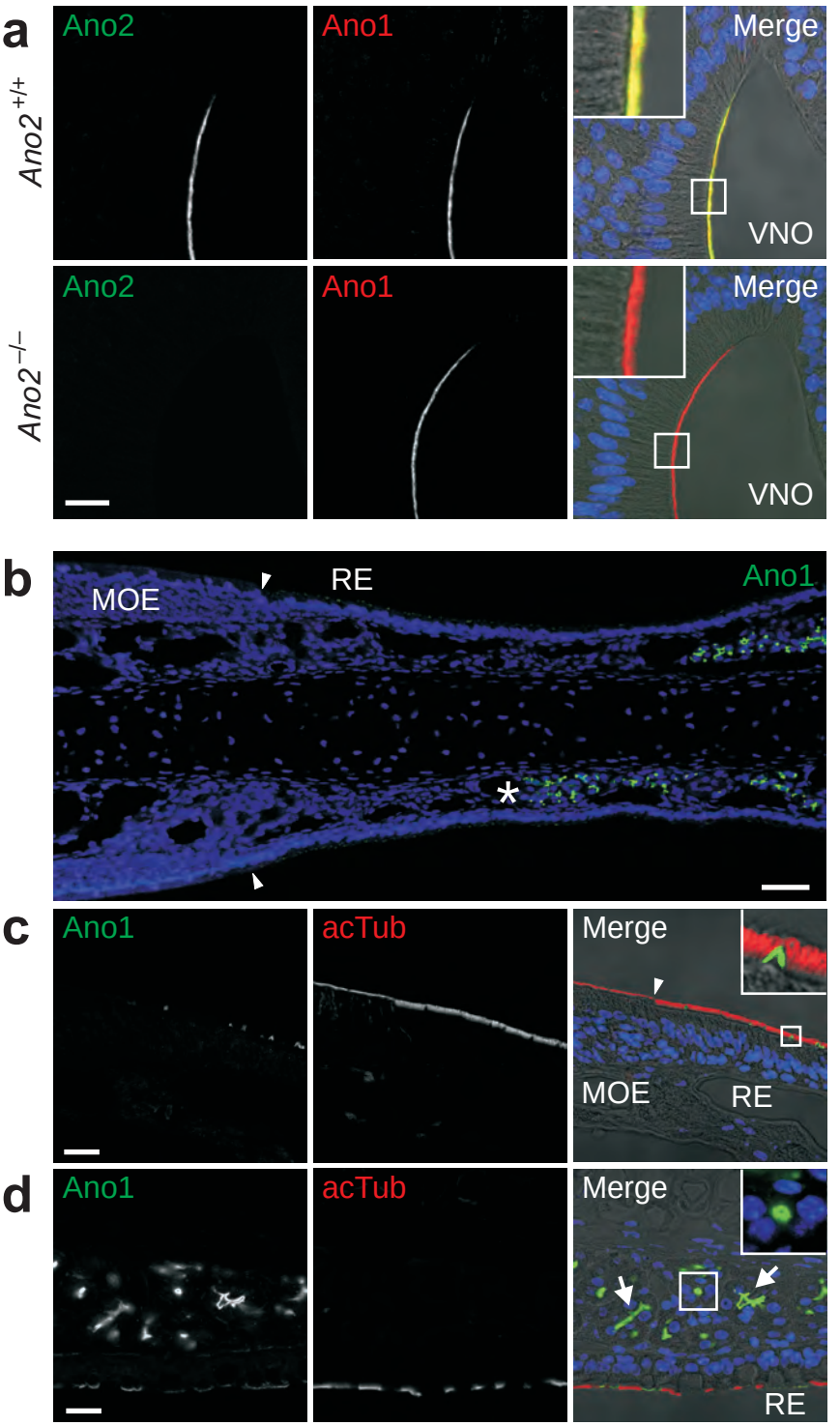

Figure 4

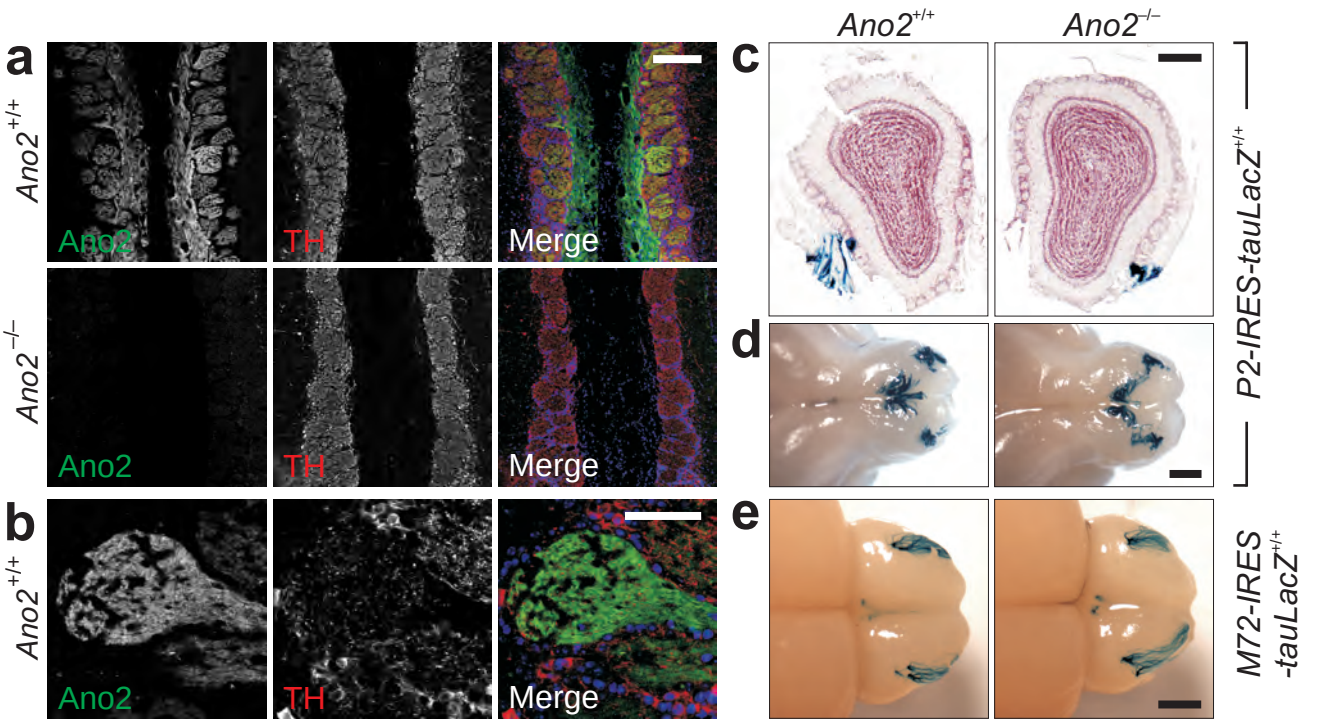
a
Ano2+/+
Ano2
TH
Merge
Ano2–/–
Ano2
TH
Merge
b
Ano2+/+
Ano2
TH
Merge
c
Ano2+/+
Ano2–/–
d
e
P2-IRES-tauLacZ+/+
M72-IRES-tauLacZ+/+

Figure 5

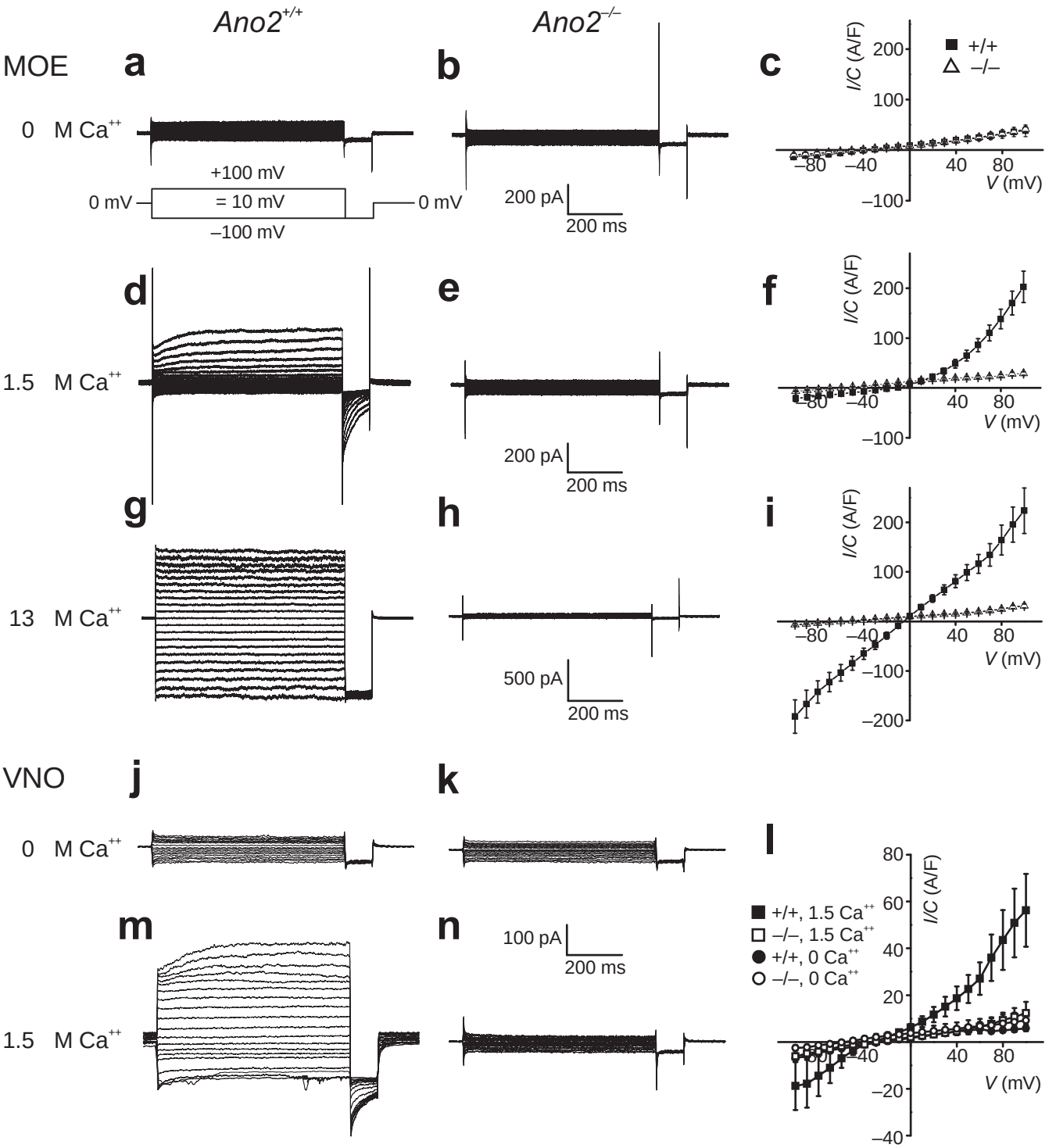
Ano2+/+
Ano2–/–
MOE
a
b
c
0 M Ca++
+100 mV
0 mV
= 10 mV
0 mV
–100 mV
200 pA
200 ms
I/C (A/F)
+/+
–/–
V (mV)
d
e
f
1.5 M Ca++
g
h
i
13 M Ca++
500 pA
VNO
j
k
l
m
n
100 pA
+/+, 1.5 Ca++
–/–, 1.5 Ca++
+/+, 0 Ca++
–/–, 0 Ca++

Figure 6

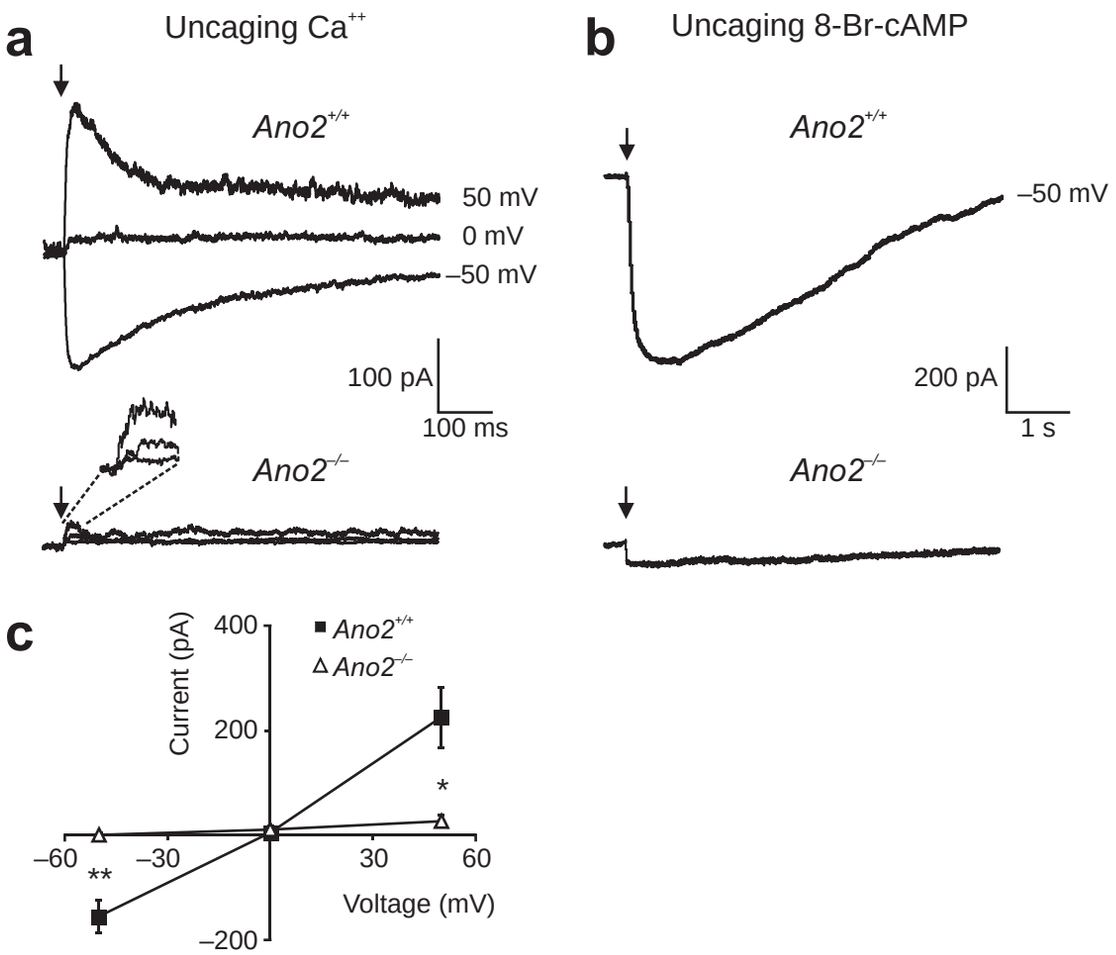
a
Uncaging Ca++
Ano2+/+
50 mV
0 mV
–50 mV
100 pA
100 ms
Ano2–/–
b
Uncaging 8-Br-cAMP
Ano2+/+
–50 mV
200 pA
1 s
Ano2–/–
c
Current (pA)
400
200
–200
–60
–30
30
60
Voltage (mV)
Ano2+/+
Ano2–/–
*
**

Figure 7

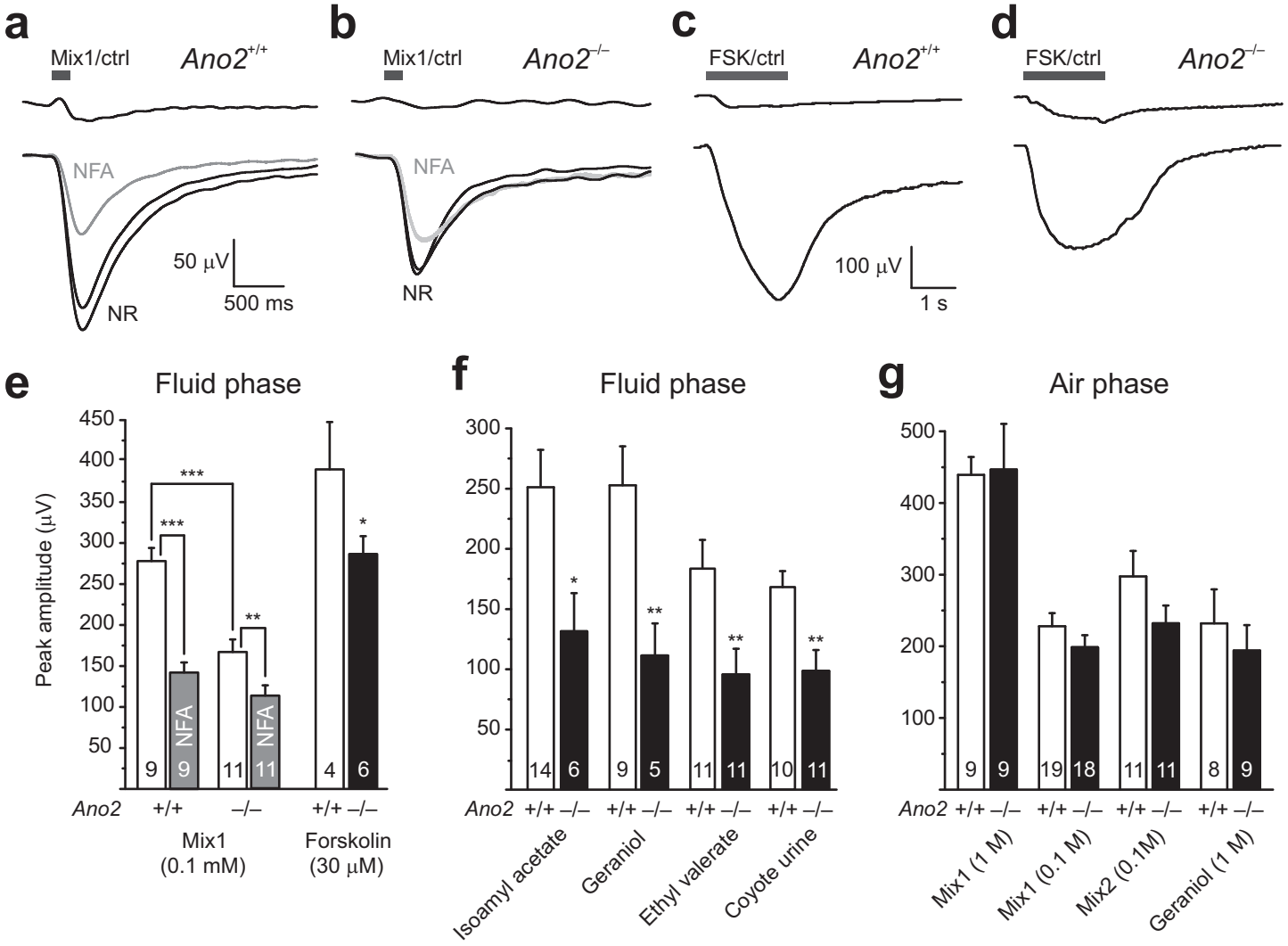
a
Mix1/ctrl
Ano2+/+
NFA
NR
50 μV
500 ms
b
Mix1/ctrl
Ano2–/–
NFA
NR
c
FSK/ctrl
Ano2+/+
100 μV
1 s
d
FSK/ctrl
Ano2–/–
e
Fluid phase
Peak amplitude (μV)
NFA
Ano2 +/+ –/– +/+ –/– +/+ –/–
Mix1 (0.1 mM)
Forskolin (30 μM)
f
Fluid phase
Ano2 +/+ –/– +/+ –/– +/+ –/– +/+ –/–
Isoamyl acetate
Geraniol
Ethyl valerate
Coyote urine
g
Air phase
Ano2 +/+ –/– +/+ –/– +/+ –/– +/+ –/–
Mix1 (1 M)
Mix1 (0.1 M)
Mix2 (0.1M)
Geraniol (1 M)

Figure 8

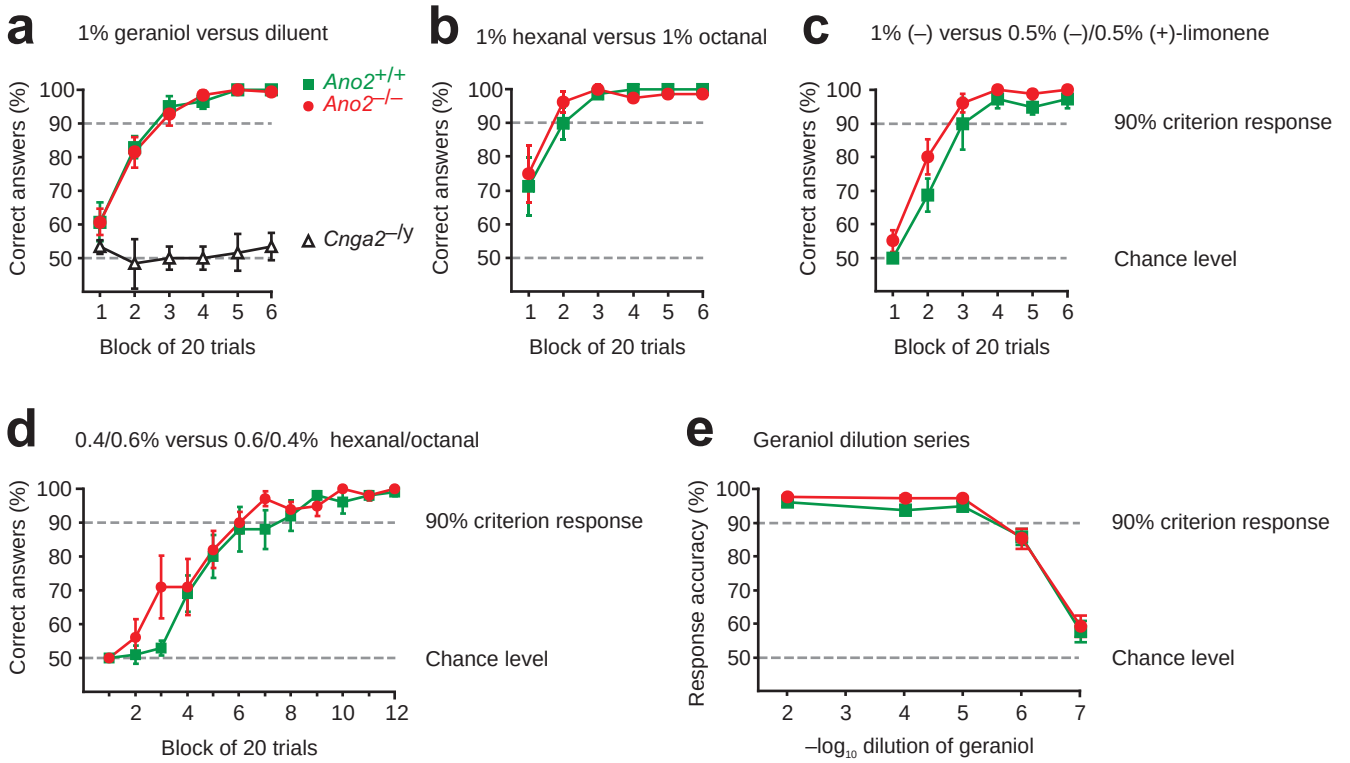
a
1% geraniol versus diluent
Ano2+/+
Ano2–/–
Cnga2–/y
Correct answers (%)
Block of 20 trials
b
1% hexanal versus 1% octanal
Correct answers (%)
Block of 20 trials
c
1% (–) versus 0.5% (–)/0.5% (+)-limonene
Correct answers (%)
Block of 20 trials
90% criterion response
Chance level
d
0.4/0.6% versus 0.6/0.4% hexanal/octanal
Correct answers (%)
Block of 20 trials
90% criterion response
Chance level
e
Geraniol dilution series
Response accuracy (%)
–log10 dilution of geraniol
90% criterion response
Chance level